Turk Neurosurg 35(6):899-913, 2025
DOI: 10.5137/1019-5149.JTN.48410-25.2

Original Investigation

Cerebrovascular-Endovascular

Received: 11.01.2025
Accepted: 09.04.2025
Published Online: 30.10.2025

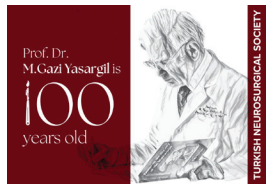

Three Dimensional Geometrical Features of Intracranial Saccular Aneurysms at the Time of Rupture

Abdel Rahman SADEK, Abdallah HASSAN, Omar ARAFA, Ahmed SULTAN, Mohamed AGAMY, Waseem AZIZ, Alaa EL NAGGAR, Tamer HASSAN

Department of Neurosurgery, Alexandria University School of Medicine, Azarita Medical Campus, Alexandria, Egypt

Corresponding author: Tamer HASSAN ✉ tamer.shihata@alexmed.edu.eg, neurocatheter@gmail.com

ABSTRACT

AIM: To explore the interplay between different geometric features of various types of aneurysms related to aneurysm rupture angiographically.

MATERIAL and METHODS: Three dimensional (3D) digital subtraction angiography (DSA) studies from 180 patients with ruptured sidewall (SW) and sidewall with branching vessel (SWB) aneurysms, and 70 patients with ruptured endwall (EW) aneurysms were retrospectively analyzed, excluding anterior communicating artery aneurysms. In SW and SWB cases, relationships between maximum aneurysm depth and various geometric features, including neck diameter, parent vessel (PV) curvature angle, and diameter difference between proximal and distal PV segments, were explored. In EW cases, the neck diameter, branching angle, and discrepancy between daughter vessel diameters were measured and compared with aneurysm depth.

RESULTS: A narrow PV curvature angle significantly correlated with greater maximum aneurysm depth in SW aneurysms (p-value=0.019). PV stenosis distal to SW aneurysms was significantly associated with greater aneurysm depth at the time of rupture (p-value<0.001). A wider branching angle was associated with smaller aneurysm depth at the time of rupture in EW aneurysms having daughter vessels narrower in caliber than their PV (p-value=0.02). A positive significant correlation was recorded between aneurysm depth and neck width in both EW and SW aneurysm types (p-value<0.001).

CONCLUSION: Geometric factors such as PV curvature angle, neck width, and PV distal narrowing could affect the risk of growth and rupture of SW and SWB aneurysms. A wider branching angle could be considered in the early rupture of EW aneurysms. Neck width could be significantly related to the growth and rupture of both SW and EW intracranial aneurysms.

KEYWORDS: Aneurysm rupture, Flow dynamics, Parent vessel curvature angle, Branching angle, Neck

ABBREVIATIONS: 3D: Three-dimensional, **AcoA:** Anterior communicating Artery, **AICA:** Anterior inferior cerebellar artery, **CFD:** Computational fluid dynamics, **DSA:** Digital subtraction angiography, **EW:** Endwall, **IA:** Intracranial aneurysm, **ICA:** Internal carotid artery, **MCA:** Middle cerebral artery, **PCA:** Posterior cerebral artery, **PcoA:** Posterior communicating Artery, **PICA:** Posterior Inferior Cerebellar Artery, **PV:** Parent Vessel, **SW:** Sidewall, **SWB:** Sidewall with Branching Vessel, **VA:** Vertebral Artery, **WNA:** Wide Neck Aneurysm

Abdel Rahman SADEK : 0009-0001-3213-8907
Abdallah HASSAN : 0009-0004-0974-664X
Omar ARAFA : 0000-0001-5075-540X
Ahmed SULTAN : 0000-0002-8733-9634
Mohamed AGAMY : 0000-0002-8402-1137
Waseem AZIZ : 0000-0002-9901-0895
Alaa EL NAGGAR : 0009-0002-6219-6929
Tamer HASSAN : 0000-0003-2136-7875

INTRODUCTION

Rupture of intracranial aneurysms (IAs) results in considerable morbidity and mortality, affecting around 2 to 5% of the total population (8). The risks of IA rupture are classified into patient-related and aneurysm-related factors. According to previous studies, patient-related factors include female sex, hypertension, current smoking status, familial preponderance, and connective tissue disorders (49,52,53). However, these investigations have not yielded any quantitative findings that are easy to incorporate into the decision-making process for IA management. Aneurysm-related rupture risk factors include geometric features such as aneurysm size (47), size ratio (8,45), shape (17,33,34), neck diameter (33), and aspect ratio (30,44). There is ongoing debate on which morphological trait best predicts a higher risk of aneurysmal rupture. Both geometric and hemodynamic factors play a major role in IA development, growth, and rupture. In the absence of underlying disease, aneurysm development is assumed to be a mechanically mediated process (11). Why some aneurysms rupture at small sizes while others grow to reach a large size in the absence of obvious abnormal angioarchitecture is still not understood. Figure 1 shows a ruptured sidewall (SW) blister aneurysm arising from a nearly straight vessel increased in both the neck and the depth dimensions after 1 month.

Regarding SW aneurysms, few studies have examined the relationship between the curvature of the parent vessel (PV) and aneurysm growth and rupture (21). Piccinelli et al. stated that greater angles at ICA curves harboring aneurysms are more likely to be associated with rupture status (32). The role of PV curvature, in the absence of a bifurcation, has not been extensively evaluated concerning SW aneurysm formation or rupture. While PV stenosis has been shown to contribute to the development and rupture (18,19), few studies have correlated PV stenosis or widening with aneurysm growth or rupture in SW aneurysms.

Regarding endwall (EW) aneurysms, a recent meta-analysis revealed that middle cerebral artery (MCA) bifurcations with wider daughter-to-daughter angles are closely associated with the formation of EW MCA bifurcation aneurysms (40). However, the relationship between the branching angle and aneurysm depth has not been explored (29).

Since studies investigating the contribution of vascular geometry to aneurysm growth and rupture are limited, we explored the correlations between geometric features in both SW and EW IAs, aiming to minimize the use of time-consuming computational fluid dynamics (CFD).

Moreover, due to the complexity and diversity of vessel geometry and flow conditions of the anterior communicating artery (AcoA) complex (6), AcoA aneurysms were excluded from our study. A normal ACA-AcoA complex is defined as one in which a communicating artery connects two A1 segments of equal size and, thus, two inflow feeder vessels, and these A1s continue upstream to form two equally sized A2 outflow draining vessels. However, AcoA aneurysms are more likely to have asymmetric A1s, and in 78% of cases, they are exclusively filled angiographically from one A1 vessel (6). This asymmetry creates variable flow patterns and, therefore, different hemodynamics that alter the risks of AcoA aneurysm rupture compared to non-AcoA aneurysms, which typically have a single inflow vessel and most often a single outflow vessel.

MATERIAL and METHODS

This study was approved according to ethical standards of scientific research by the ethics committee with reference number 12-11-2023/0108087.

Patient Population

This study involved a retrospective analysis of 250 patients with ruptured saccular IAs admitted to the neurosurgery department and affiliated hospitals. The included cases had a definitive digital subtraction angiography (DSA) result confirming a diagnosis of anterior circulation aneurysms and posterior circulation aneurysms. AcoA aneurysms were excluded.

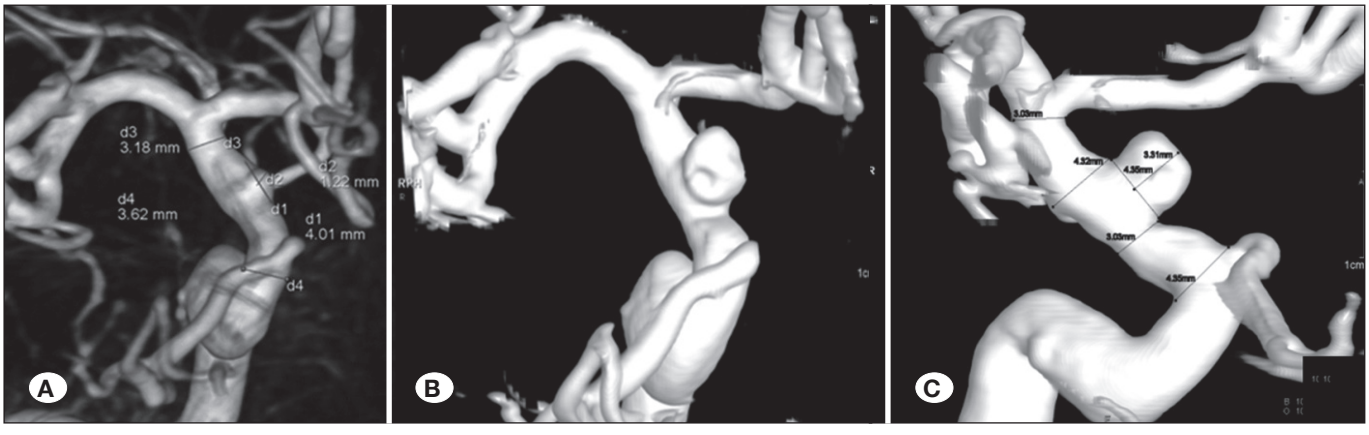

Figure 1: A) Three dimensional digital subtraction angiography image of a ruptured right dorsal ICA sidewall blister aneurysm in a 44-year-old male patient. Neck diameter=4.01 mm, maximum depth=1.22 mm. **B)** and **C)** Follow-up DSA after 1 month revealed aneurysm growth; neck diameter=4.36 mm, maximum depth=3.31 mm.

3D Image Extraction

For patients diagnosed with ruptured saccular EW, SW, or SWB IAs, images were extracted from DSA (using the Siemens Artis-Z® angiogram) as two-dimensional (2D) and three-dimensional (3D) images. The angiographic data were transported to a workstation (Syngo X Workplace; Siemens) running prototype software for the post-processing of 3D DSA images and analyzed thoroughly to obtain the 3D geometric morphological features of the aneurysms and their PVs.

Aneurysm Morphological Characteristics

Aneurysm morphological features were extracted from the DSA images. A blinded image review was performed and the aneurysm location and the age and sex of the patients were recorded.

All saccular aneurysms were classified as SW, EW, or SWB based on the recorded angiographical patterns of parent arteries, according to Hassan et al. SW aneurysms are characterized by the aneurysm's inflow and outflow zones being located within the same anatomical neck, with the aneurysmal sac arising from a single vessel, which acts as both the feeding and the draining channel (13). SWB aneurysms are geometrically similar to SW aneurysms, except that the aneurysm sac is connected to additional draining arteries (13). In EW aneurysms, the diameter of the PV proximal to the aneurysm is separated from the greatest diameter of the PV distal to the aneurysm by less than 90%, meaning that the mainstream of blood flow enters the aneurysm (13).

Aneurysm measurements of maximal diameter were obtained as the maximum height or depth. This is not the height measured perpendicularly, but rather the maximum (and not always perpendicular) distance between any location on the aneurysm dome and the centroid of the aneurysm neck. As accurately as possible, the neck plane was identified as the point at which the aneurysmal sac protruded from the PV.

SW Aneurysms

Average PV diameter(s) (pre- and post-aneurysm) were recorded in both the proximal pre-aneurysm segment and the distal post-aneurysm segment. For each segment, two representative vessel cross-sections were obtained: the proximal neck (D1) and a point 1.5 times upstream (D2). The average value of these measurements was then calculated. The absolute difference between the pre- and post-aneurysm PV average diameters was also calculated. Additionally, the PV curvature angle was measured. This angle was measured between two lines: one passing through the longitudinal axis of the PV segment proximal (inflow) to the aneurysm neck and the other through the longitudinal axis of the PV segment distal (outflow) to the aneurysm neck. The angle measured was the internal angle formed by the intersection of these lines at the centroid of the aneurysm neck, ensuring that the angle was measured from the direction where the proximal segment, distal segment, and aneurysm were observed in the same plane. SW and SWB aneurysm measurements are shown in Figures 2 and 3.

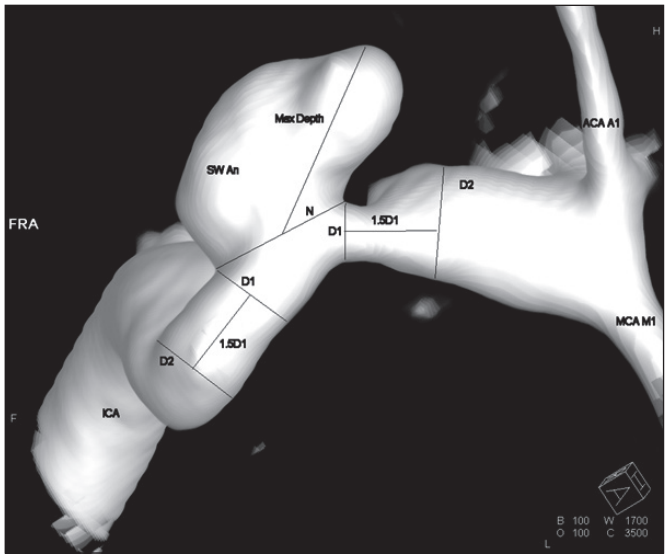

Figure 2: Representative 3D DSA image of a sidewall aneurysm of the left internal carotid artery ophthalmic segment in a 34-year-old female patient. N=neck diameter. Max depth=maximum aneurysm depth. For each parent vessel segment, D1=parent vessel diameter at the proximal neck, D2=parent vessel diameter at 1.5D1 upstream of the aneurysm, ICA=internal carotid artery, ACA A1=A1 segment of the anterior cerebral artery, MCA M1=M1 segment of the middle cerebral artery.

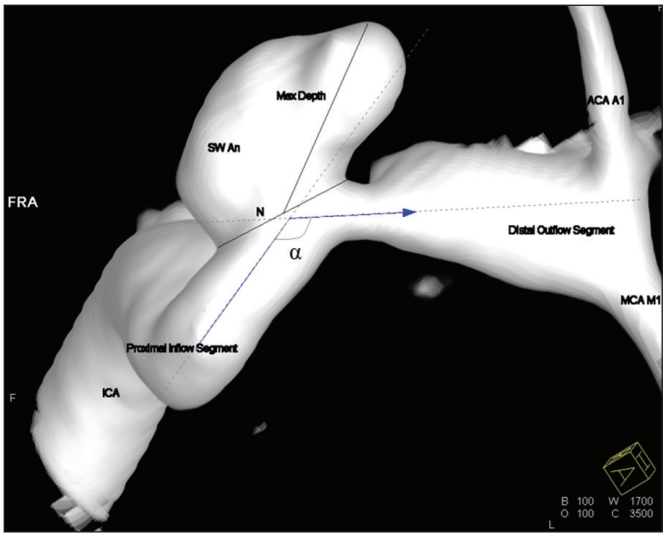

Figure 3: Representative 3D DSA image of a sidewall aneurysm of the left internal carotid artery ophthalmic segment in a 34-year-old female patient. The parent vessel curvature angle (α) between the proximal inflow and distal outflow segments is represented by the blue arrow formed by the intersection of the longitudinal axes (dotted lines) of both segments. The arrowhead represents the direction of blood flow. N=neck diameter, ICA=internal carotid artery, ACA A1= A1 segment of the anterior cerebral artery, MCA M1=M1 segment of the middle cerebral artery.

EW (Bifurcation) Aneurysms

Average PV diameters were obtained by measuring two representative cross-sections of the PV (Pa1 at the PV terminus and Pa2 1.5 times upstream of Pa1) and calculating their average value. The average diameter of each daughter artery was measured using the same method: two representative vessel cross-sections upstream of the aneurysm (the proximal neck, D1, and a point 1.5 times upstream, D2) were measured and averaged. The difference in diameter between the daughter arteries was then calculated. Additionally, the absolute difference between the average diameter of the parent artery and the average diameter of the daughter arteries was calculated. The branching angle was also recorded by measuring the internal angle between two lines running through the longitudinal axis of each daughter vessel. EW aneurysm measurements are shown in Figures 4 and 5.

Statistical Analysis

For the primary estimations and case collection, a Microsoft Excel 2023 spreadsheet with statistical tools was used. The IBM SPSS software package version 20.0 (IBM Corp., Armonk, NY, USA) was used for all additional statistical analyses. The statistical significance of the correlations between the aneurysm maximum depth and other parameters, such as PV curvature angle and aneurysm neck diameter, was determined using linear regression analysis. The dimensions of the aneurysm were measured using 3D DSA images, where the maximum value of each measured parameter (neck diameter, maximum aneurysm depth, and PV diameter) defined the aneurysm's dimensions. Each PV measurement was made with the longitudinal vessel axis perpendicular to the measurement. Calculations were performed to determine the coefficient of determination and the error probability values. Significant probability values were those less than 0.05. Graphical representations of the results were created using bivariate scatter plots and regression. Numbers and percentages were used to describe the qualitative data. To verify the normality of the distribution, the Shapiro–Wilk test was performed. Range (minimum and maximum), mean, standard deviation, median, and interquartile range (IQR) were used to characterize quantitative data.

RESULTS

A total of 250 cases of ruptured saccular IAs, excluding AcoA aneurysms, were collected from neurosurgery department hospitals and affiliated hospitals, with a mean patient age of 51.2 ± 14.1 years. More than 50% of patients were female (133; 53.2%), and 58% of the patients were aged ≥50 years. Table I summarizes the demographic data of the collected sample. The 250 aneurysms were classified angiographically based on their PV geometry into EW, SW, and SWB types. About 53% (132 out of 250) of the cases were SW, 28% were EW, and 19% were SWB aneurysms. Regarding aneurysm location, most cases were PcoA aneurysms (69; 27.6%), fol-

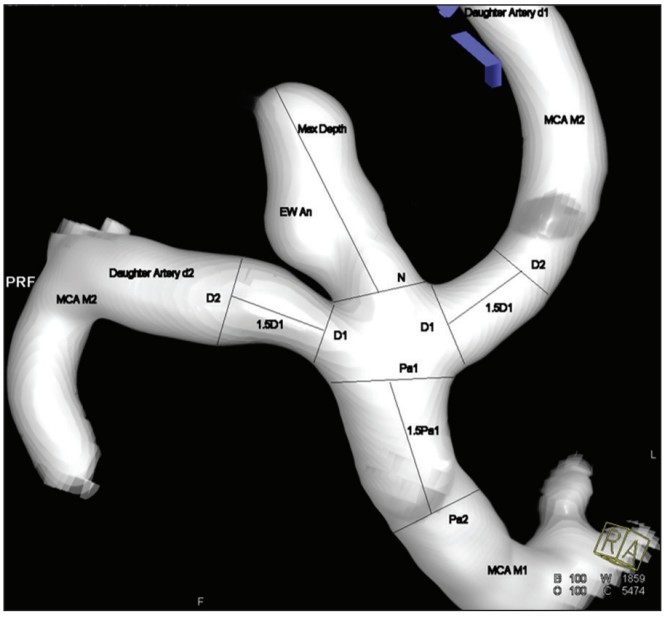

Figure 4: Representative 3D DSA image of an endwall aneurysm arising from the right middle cerebral artery bifurcation in a 62-year-old male patient. N=neck diameter. Max depth=maximum aneurysm depth. For each daughter artery d1 and d2, D1=vessel diameter at the proximal neck, D2=vessel diameter at 1.5D1 upstream of the aneurysm, Pa1=parent vessel diameter at the parent vessel terminus, Pa2=parent vessel diameter at 1.5Pa1 upstream, MCA M1=M1 segment of the middle cerebral artery, MCA M2=M2 segment of the middle cerebral artery.

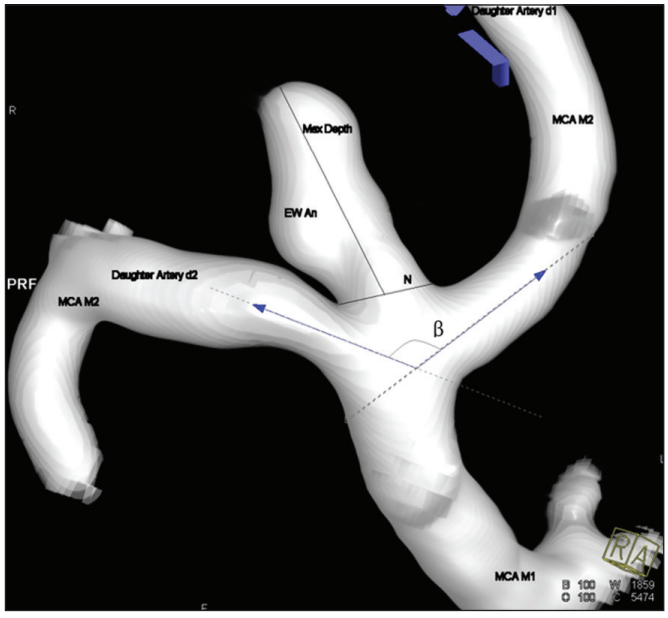

Figure 5: Representative 3D DSA image of an endwall aneurysm (EW An) arising from the right middle cerebral artery bifurcation in a 62-year-old male patient. The branching angle (β) is formed by the intersection of the longitudinal axis of each daughter vessel (two dotted lines on d1 and d2). Blue arrowheads represent the direction of blood flow. Neck diameter=2.23 mm. N=neck diameter, Max depth=maximum aneurysm depth, MCA M1=M1 segment of the middle cerebral artery, MCA M2=M2 segment of the middle cerebral artery.

Table I: Distribution of the Studied Cases according to Demographic Data (n=250)

	No.	%
Sex		
Male	117	46.8
Female	133	53.2
Age (years)		
<50	105	42.0
≤50	145	58.0
Min. – Max.	11.0-76.0	
Mean ± SD.	51.16 ± 14.05	
Median (IQR)	53.0	

***IQR:** Inter quartile range, **SD:** Standard deviation.*

lowed by ophthalmic segment ICA aneurysms (52; 20.8%) and MCA bifurcation aneurysms (45; 18%). Table II classifies the studied aneurysms within PV geometry-related categories and presents the range, mean, and median values of the measured parameters for each aneurysm location. In all 250 cases, the maximum aneurysm depth measured at the point of rupture was 6.26 ± 4.16 mm, and the average aneurysm neck diameter was 3.68 ± 1.7 mm.

SW Aneurysms

Regarding SW and SWB aneurysms, Table III presents a descriptive analysis of the parameters measured. First, a significant correlation was observed between the PV curvature angle and the maximum aneurysm depth at which rupture occurred, with statistical significance (p-value=0.019). Figures 6, 7, and 8 show 2D scatter plots of the observed correlation between the different morphological parameters measured in 180 SW and SWB aneurysms. Second, a significant correlation was

Table II: Classification of Studied Aneurysms According to Location and Parent Vessel Geometry-Related Categories

No. of Aneurysms (%)				Morphological Parameters					
				Aneurysm Max Depth			Neck size		
Aneurysm location	SW Sidewall	SWB Sidewall with branching vessel	EW Endwall	Mean value ±SD	Min.-Max.	Median (IQR)	Mean value ±SD	Min.-Max.	Median (IQR)
PcoA	38	31	0	5.95 ± 3.14	1.31-14.2	5.54 (3.42-8.27)	3.38 ± 1.45	1.16-10.2	3.06 (2.38-3.85)
MCA	10	2	45	5.50 ± 2.92	1.93-19.6	4.8 (3.52-6.67)	3.56 ± 1.46	1.89-7.76	3.1 (2.44-4.1)
ICA Ophthalmic segment	45	7	0	6.28 ± 5.12	0.83-23.4	4.91 (2.94-7.23)	3.89 ± 2.17	1.5-13.7	3.31 (2.36-4.71)
ACA	8	2	6	4.19 ± 2.262	0.93-9.07	3.56 (2.64-5.93)	2.71 ± 1.29	0.93-5.17	2.54 (2.03-3.02)
Other CA	23	4	10	8.33 ± 5.48	2.11-27.8	6.16 (3.94-11.9)	4.39 ± 1.69	1.38-8.76	4.27 (3.23-5.0)
PCA	3	0	0	11.26 ± 8.64	3.56-20.6	9.62 (6.59-15.11)	4.64 ± 1.55	3.27-6.33	4.33 (3.8-5.33)
BA	0	0	9	6.81 ± 3.84	2.24-13.9	7.3 (4.09-8.61)	4.59 ± 1.86	1.8-8.09	4.91 (3.34-5.25)
PICA	2	1	0	5.18 ± 2.51	2.51-7.5	5.52 (4.02-6.51)	2.64 ± 0.46	2.25-3.15	2.51 (2.38-2.83)
AICA	1	0	0	4.78	–		2.54	–	
VA	2	1	0	5.11 ± 3.30	2.41-8.79	4.14 (3.28-6.47)	3.29 ± 0.64	2.55-3.73	3.59 (3.07-3.66)
Total (n=250)	132 (52.8)	48 (19.2)	70 (28)	6.26 ± 4.16	0.83-27.80	5.22 (3.5-7.6)	3.68 ± 1.70	0.93-13.70	3.25 (2.5-4.5)

***PcoA:** Posterior communicating artery, **MCA:** Middle cerebral artery, **ICA:** Internal carotid artery, **ACA:** Anterior cerebral artery, **CA:** Carotid artery, **PCA:** Posterior cerebral artery, **BA:** Basilar artery, **PICA:** Posterior inferior cerebellar artery, **AICA:** Anterior inferior cerebellar artery, **VA:** Vertebral artery, **IQR:** Inter quartile range, **SD:** Standard deviation.*

Table III: Descriptive Analysis of the Studied Cases According to Different Morphological Parameters in Sidewall (SW) and Sidewall with Branching Vessel (SWB) Saccular Aneurysms (n=180)

Morphological Parameter	SW and SWB (mean value ± SD)
Maximum Depth (mm)	6.34 ± 4.44
Neck Diameter (mm)	3.63 ± 1.74
Pre-Aneurysm parent vessel diameter at neck (D1) (mm)	2.86 ± 1.03
Pre-Aneurysm parent vessel diameter at 1.5xD1 (D2) (mm)	3.15 ± 1.08
Proximal (inflow) parent vessel average diameter (D1+D2/2) (mm)	3.00 ± 1.00
Post-Aneurysm parent vessel diameter at neck (D1) (mm)	2.88 ± 0.97
Post-Aneurysm parent vessel diameter at 1.5D1 (D2) (mm)	2.82 ± 0.92
Distal (outflow) parent vessel average diameter (D1+D2/2)(mm)	2.85 ± 0.88
Parent vessel curvature angle (deg)	109.2 ± 28.4
Parent vessel diameter difference between proximal and distal segments	0.45 ± 0.44

SD: *Standard deviation.*

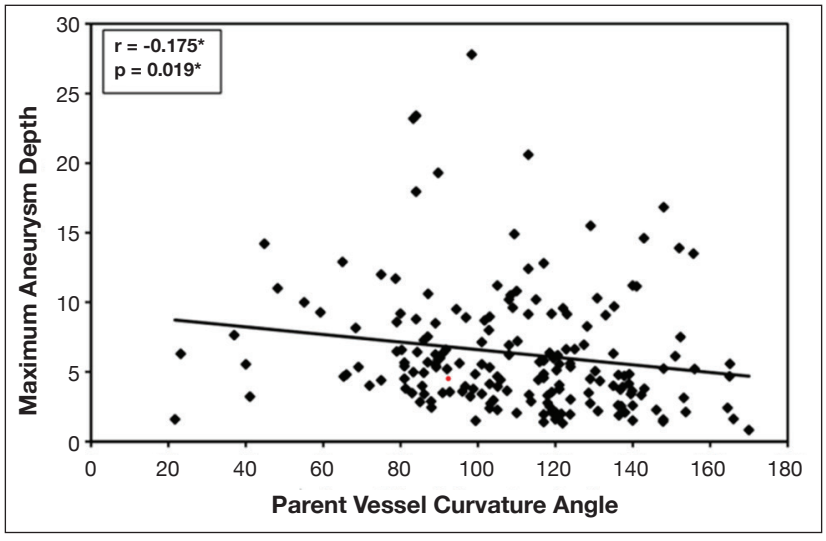

Figure 6: 2D scatter plot showing a correlation between parent vessel curvature angle and maximum depth in SW and SWB saccular aneurysms (n=180). ***=**statistically significant.

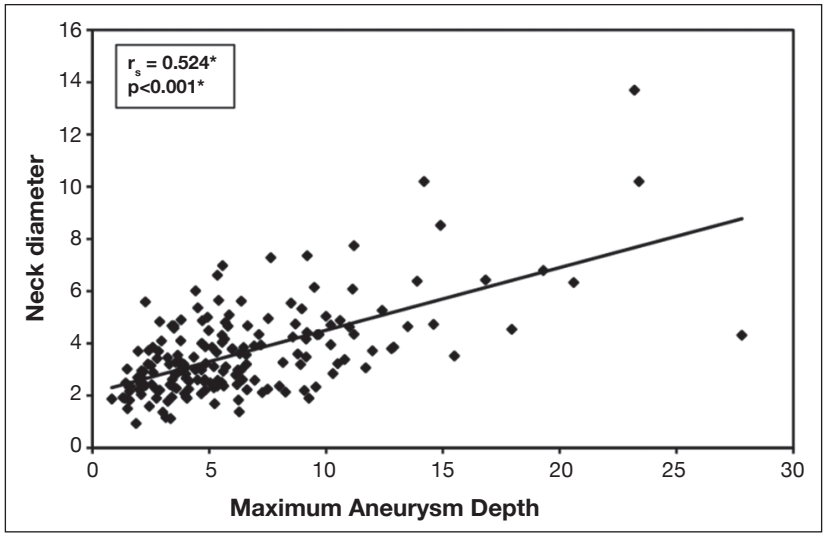

Figure 7: 2D scatter plot showing a correlation between neck diameter and maximum depth in SW and SWB saccular aneurysms (n=180). ***=**statistically significant.

found between neck diameter and maximum aneurysm height at which rupture occurred, with statistical significance (p-value<0.001). Regarding the discrepancy between proximal and distal PV segments, in 60% of the cases (n=180 SW and SWB aneurysms), the distal PV segment was found to be narrower than the proximal segment. Cases with distal narrowing of the parent artery showed a significant correlation between proximal and distal segment discrepancy and the maximum depth at which the aneurysm ruptured (p-value<0.001), as shown in Table IV and Figures 9 and 10. The greater the difference in caliber between the proximal and distal segments, the greater the aneurysm size. However, cases with proximal narrowing of the PV showed no statistically significant correlation between segment discrepancy and the maximum aneurysm depth (p-value=0.75).

EW Aneurysms

Regarding EW aneurysms, Table V summarizes the measured parameters. A significant correlation was recorded between aneurysm neck diameter and maximum aneurysm depth at which rupture occurred (p-value<0.001) as shown in Figure 11. However, no statistically significant correlation was found between the daughter vessel caliber discrepancy and the maximum aneurysm depth. Regarding the branching angle, no significant relationship was noted between the branching angle and the maximum aneurysm depth at which rupture occurred. However, a subgroup analysis of the 70 EW aneurysms was performed based on the difference in vessel caliber between the PV and the average of the two daughter vessels. A total of 62 out of 70 EW aneurysms (89%) had PV diameters larger than the average daughter vessel diameters. This subgroup showed a statistically significant inverse correlation between the branching angle and the maximum aneurysm depth at the time of rupture (p-value=0.02). Figures 12 and 13 show 2D scatter plots of the observed correlation between different morphological parameters measured in 70 EW aneurysms. Ta-

Table IV: Univariate Analysis of the Studied Cases according to Parent Vessel Diameter Difference Between Proximal and Distal Segments in (SW) and (SWB) Aneurysms (n=180) (*=statistically significant)

Stenotic Parent Vessel Segment	n (%)	Parent vessel Diameter Difference between proximal and distal segment (mean in mm ±SD)	Maximum Aneurysm Depth (mean in mm)	p-value
Distal Segment	106 (58.9)	0.51 ± 0.48	6.59 ± 4.95	<0.0001*
Proximal Segment	72 (40)	0.37 ± 0.35	5.96 ± 3.61	0.75
Distal=Proximal	2 (0.01)	0	6.96	----

SD: *Standard deviation.*

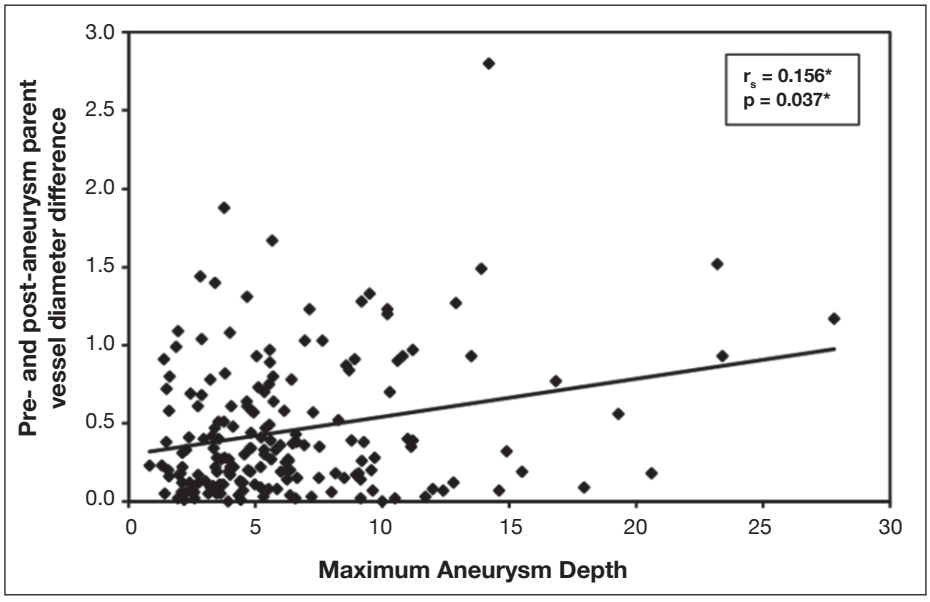

Figure 8: 2D scatter plots showing a correlation between absolute pre- and post-aneurysm parent vessel diameter difference and maximum depth in SW and SWB saccular aneurysms (n=180). ***=**statistically significant.

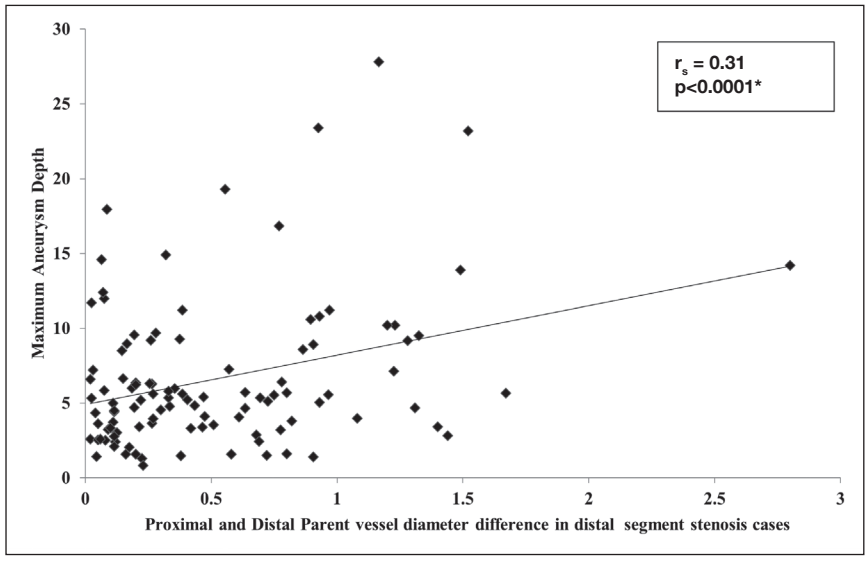

Figure 9: 2D scatter plot showing a correlation between pre- and post-aneurysm parent vessel diameter difference and maximum aneurysm depth in SW and SWB aneurysms with PV distal segment stenosis (n=106). *=statistically significant.

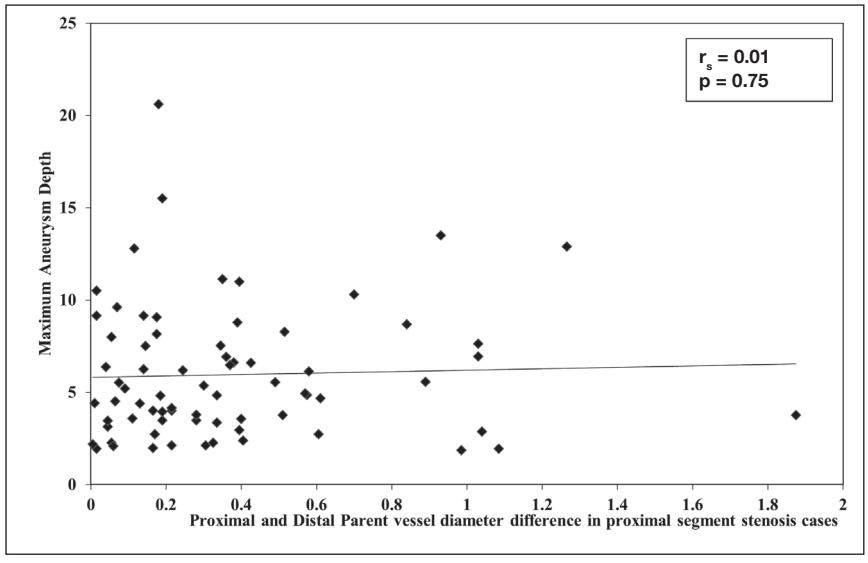

Figure 10: 2D scatter plot showing a correlation between pre- and post-aneurysm parent vessel diameter difference and maximum aneurysm depth in SW and SWB aneurysms with PV proximal segment stenosis (n=72).

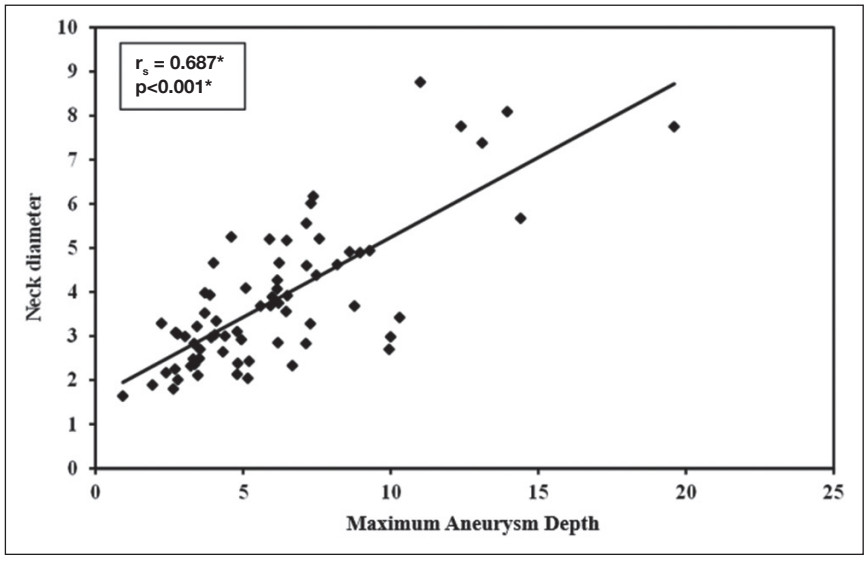

Figure 11: 2D scatter plot showing a correlation between neck diameter and maximum aneurysm depth in EW aneurysms (n=70). *=statistically significant.

Table V: Descriptive Analysis of the Studied Cases according to Different Morphological Parameters in Endwall Saccular Aneurysm (n=70)

Morphological Parameter	EW (mean value ± SD)
Maximum Depth (mm)	6.05 ± 3.35
Neck Diameter (mm)	3.81 ± 1.60
Parent vessel diameter (mm)	2.42 ± 0.62
Daughter vessel diameter d1 (mm)	1.77 ± 0.46
Daughter vessel diameter d2 (mm)	1.74 ± 0.48
Average Daughter vessels diameter (d1+d2/2) (mm)	1.76 ± 0.38
Branching Angle (deg)	119.5 ± 33.2
Daughter vessels diameter difference (mm)	0.44 ± 0.35
Parent-Daughter vessel diameter difference (mm)	0.72 ± 0.49

SD: *Standard deviation.*

Table VI: Correlation Between Branching Angle and Maximum Aneurysm Depth in Subgroup Analysis of the Studied (EW) Aneurysms According to Parent-Daughter Vessel Ratio (n=70) (*=statistically significant)

Parent-Daughter vessel ratio	n (%)	Branching angle (mean in deg ± SD)	Maximum Aneurysm Depth (mean in mm)	p-value
Parent>Daughter	62 (89)	121.5 ± 31.3	6.11 ± 3.35	0.02*
Parent<Daughter	8 (11)	102.1 ± 41.7	5.59 ± 3.26	0.75

SD: *Standard deviation.*

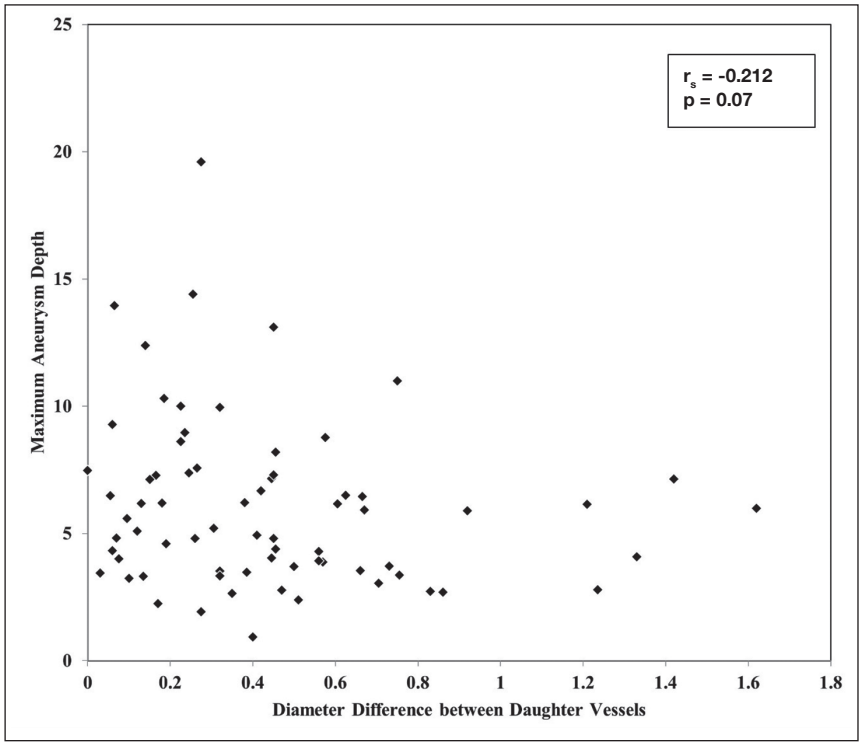

Figure 12: 2D scatter plot showing a relationship between daughter-daughter vessel diameter difference and maximum aneurysm depth in EW aneurysms (n=70).

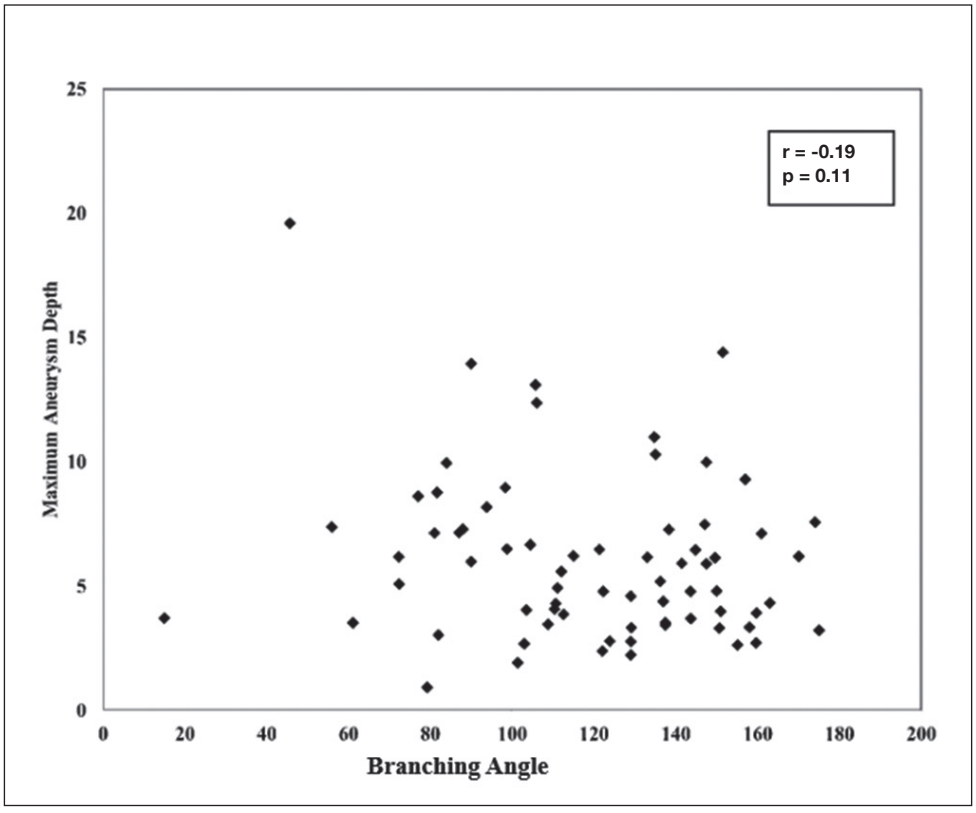

Figure 13: 2D scatter plot showing a relationship between branching angle and maximum aneurysm depth in EW aneurysms (n=70).

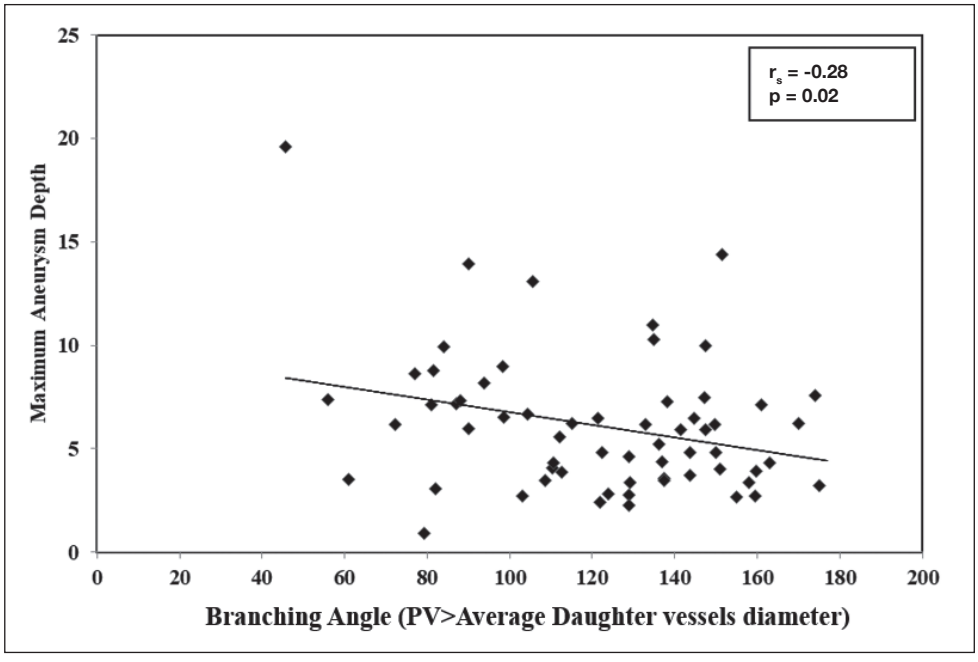

Figure 14: 2D scatter plot showing a correlation between branching angle and maximum aneurysm depth in EW aneurysm cases with a parent vessel diameter larger than the average of both daughter vessel diameters (n=62).

ble VI and Figure 14 show the significant correlation between the daughter-to-daughter branching angle and the maximum aneurysm depth.

DISCUSSION

The present study focused on 250 ruptured IAs to explore different geometric parameters that could be used to anticipate aneurysmal rupture. Most studies that compare ruptured and unruptured aneurysms face similar difficulties. There is ongo-

ing debate about the aneurysmal morphological changes that might occur at rupture. For this reason, conducting prospective analysis for unruptured aneurysms is challenging. Recent prospective studies have incorporated vessel imaging modalities such as black blood contrast-enhanced MRI to help detect inflammatory changes in the aneurysm wall that occur before rupture (9,41). Additionally, identifying which unruptured aneurysms are vulnerable to rupture remains difficult due to the inconsistent results of various studies comparing risk factors for aneurysm rupture between ruptured and unruptured groups. One reason for this difficulty is the inability to control confounding factors related to the patient characteristics affecting the risk of rupture, such as gender, age, hypertension, and current smoking status. Several studies avoided such confounding factors by comparing parameters of ruptured and unruptured aneurysms within the same patient among patients having multiple IAs (4,31).

Hemodynamic disparities between ruptured and unruptured IAs have been extensively studied using medical image-based CFD methods, contributing to the recognition of variable hemodynamic parameters that predict the likelihood of aneurysm rupture (5,50). However, our study addressed easily extracted simple geometric parameters that could add value to risk stratification regarding aneurysmal growth and rupture.

Neck Size

The most consistent risk factor for aneurysm rupture, according to previous research, is the aneurysm size (7). An increased risk of rupture has previously been linked to an aneurysm size greater than 7 mm (42,48). However, in our study, 174 (69.9%) out of the total 250 ruptured IAs had a maximum aneurysm height of less than 7 mm, and the average maximum height was 6.26 ± 4.16 mm, indicating that aneurysm size alone is not reliable for rupture risk assessment. That is why another significant geometric parameter was incorporated, that is, neck size. In 1994, Fernandez Zubillaga et al. defined neck size as the maximum size in millimeters of the aperture connecting the parent artery to the aneurysm body (10). The neck region is a critical factor that controls the blood flow into and out of the aneurysmal sac and is directly related to the speed of blood flow into the aneurysm (37,45).

The present study revealed that neck size was significantly correlated with the maximum depth at which rupture occurred in both SW and EW aneurysms with p-values <0.001. A wider neck size allows more blood flow into the aneurysmal sac, enabling the aneurysm to grow to a greater depth without early rupture. Regarding the management of IAs, wide neck aneurysms (WNAs; neck diameter ≥4 mm (10)) are considered more difficult to manage than narrow neck aneurysms (14). Due to the surgical challenges posed by WNAs and the risk of perforator injury, WNAs are considered candidates for open surgery to achieve complete and permanent aneurysm occlusion. However, the endovascular management of WNA using simple coil embolization is also difficult (23). Considering our results, the risk of WNAs attaining large sizes is higher compared to narrow neck aneurysms, thus presenting a greater risk of incomplete aneurysm occlusion, coil protrusion into the parent artery, and recanalization of the previously coiled aneurysm. Therefore, simple embolization of WNA without the use of adjunctive devices, as in balloon-assisted coiling, stent-assisted coiling, or flow divertors, is extremely difficult (34).

PV Curvature Angle

In 180 cases of SW and SWB ruptured saccular IAs, narrowing of the PV curvature angle was found to be associated with aneurysm rupture at a greater aneurysm depth. The more acute the bending angle of the PV, the larger the aneurysm depth at which rupture occurred. According to a study of flow dynamics on canine models, there is a significant difference in flow mechanisms between aneurysms arising from straight and curved PVs (28). It has also been established that changes in the blood flow trajectory caused by the bending of the PV are related to the initial endothelial effects involved in the formation or growth of the aneurysmal sac (46). Our results revealed that the more the PV bends, the greater the size attained by the aneurysm as more blood enters the aneurysm sac, leading to greater aneurysm growth. Useful information has been extracted from the effect of widening the PV curvature angle to manage SW and SWB aneurysms located on highly curved vessels using flow diverter stents. According to Janot et al., the increase of parent artery straightening— essentially, making a more obtuse branching angle—after flow diverter stent deployment favors higher rates of aneurysm occlusion (16). According to Gao et al., stent-assisted aneurysm embolization reduces the flow impingement zone at the aneurysm neck by widening the PV angle (12). Ishii et al. found that the aneurysm recurrence rate is reduced when the PV angle is raised over 20° using stent-assisted coil embolization (15). Furthermore, a recent study on ICA saccular aneurysms managed by pipeline embolization devices revealed that aneurysms arising from the outer convexity of the supraclinoid segment are considered a predictor of incomplete aneurysm occlusion owing to the higher flow velocity magnitude and jet flow into the aneurysm compared to aneurysms arising from the inner concave side of the supraclinoid ICA (39). Adding these findings to our results, the narrowing of the PV in the SW aneurysm increases the likelihood of the aneurysm reaching greater sizes. Ultimately, interpreting the aneurysmal geometric morphology and the vessels in its vicinity, especially the PV geometry, before applying the treatment strategy may help decrease iatrogenic complications or retreatments (2,24). For instance, stent-assisted coil embolization may be more beneficial than simple or balloon-assisted coil embolization for a patient with a growing SW aneurysm whose PV curvature angle shows narrowing at follow-up, thus reducing the risk of aneurysm recurrence (12,15,51). A recent CFD study showed that the deformation of the PV angle caused by stent deployment reduces the wall shear stresses and the blood velocity at the entrance of the aneurysm neck, therefore decreasing the risk of recurrence (35).

Diameter Discrepancy of Proximal (Pre-aneurysm) and Distal (Post-aneurysm) PV Segments in SW and SWB Aneurysms

Variations in vessel morphology cause hemodynamic alterations that could lead to the creation and development of an IA (18,19). De novo aneurysm origination was previously

linked to vessel narrowing, which changes the original tube-like geometry (18,19,36). Samano et al. described de novo right (PcoA) SW aneurysm development and rupture in a patient previously diagnosed with right ICA atherosclerotic stenosis 11 years ago (36). In the present study, the discrepancy between the PV narrowing of the proximal (pre-aneurysm) segment and distal (post-aneurysm) segment was assessed in relation to the aneurysm size at which rupture occurred. In cases where the distal post-aneurysm segment was narrower than the proximal ones, an increase in the diameter discrepancy between the segments was concluded to result in aneurysmal rupture at greater sizes (p-value<0.0001). However, in cases where the narrow segment was the proximal pre-aneurysm segment, no statistically significant relationship was reported between the discrepancy in the caliber of pre- and post-aneurysm segments and the risk of aneurysm depth and rupture. Our study results are consistent with the firehose nozzle theory demonstrated by Lauric et al. (22). This theory describes a vessel tapering phenomenon in the A1 segment caliber, which was shown to lead to higher blood flow velocity toward the bifurcation apex, resulting in increased wall shear stress, thus creating favorable aneurysmogenic hemodynamic conditions for AcoA aneurysm initiation and progression. Our study, which included SW and SWB aneurysms (n=180) from various locations, supports the generalization of this theory beyond just AcoA or MCA aneurysms. In addition, based on our results, it is postulated that in SW aneurysms, mechanical angioplasty of the distal segment of the PV along with aneurysm coiling would help reduce the hemodynamic conditions created by distal PV tapering and prevent further aneurysm growth or recurrence. However, further research and analysis are needed to investigate the effect of angioplasty, whether mechanical using stents or medical using intraarterial vasodilators, in SW and SWB aneurysms associated with distal PV tapering.

Branching Angle in EW Aneurysms

Prior research has demonstrated the correlation between the development, growth, and rupture of IAs and surrounding vessel angles. Regarding intracranial bifurcation aneurysm development and angles, Meng et al. showed that broader angles between the posterior cerebral arteries (PCA) caused blood flow to be shifted at the basilar apex, leading to aneurysm formation (27). Patients with basilar tip aneurysms have wider bilateral PCA angles, as demonstrated by Tütüncü et al.; similarly, Baharoglu et al. discovered that patients with MCA aneurysms are more likely to have wider daughter vessel angles (2,43). Lin et al. (24), Baharoglu et al. (3), and Lv et al. (26) measured the inflow angle (the angle between the PV and aneurysm axis) to investigate the relationship between the rupture of IAs and the PV's configuration. Their investigations revealed that aneurysm rupture is related to a wider inflow angle, which increases the flow impingement zone to the aneurysm wall. Therefore, the previously studied correlations prove that IA development and rupture are closely related to the angles of surrounding vessels. However, the studies, including our study, differ in that we explored the ratio between PV diameter and the average diameter of daughter vessels and how it may affect the correlation between the branching angle and aneurysm depth at the time of rupture. Regarding EW bifurcation aneurysms, proximal narrowing causes unphysiologically high wall shear stress at the bifurcation, as demonstrated by Kono et al. on parametric and patient-derived models. This creates conditions that were previously linked to endothelial remodeling, which is related to aneurysm development (18,19). Furthermore, Antonov et al. concluded that there was a significant correlation between the probability of rupture in MCA bifurcation aneurysms and the degree and proximity of upstream M1 parent artery stenosis (1). Lauric et al. reported that M1 segments leading to EW MCA bifurcation aneurysms show a progressive decrease in caliber, not seen in nonaneurysmal contralaterals or even in healthy individuals (20).

In our study, 62 out of 70 EW aneurysms (including 40 MCA bifurcation aneurysms, nine ICA bifurcation aneurysms, five basilar tip aneurysms, and eight distal ACA aneurysms) had daughter vessels narrower than their PV, which aligns with the previously mentioned vessel narrowing theory demonstrated by Kono et al. (18,19). Moreover, the correlation between the branching angle and the aneurysm depth at which the rupture occurred was explored. A statistically significant inverse correlation (p-value=0.02) was found, indicating that the greater the angle, the greater the hemodynamic stresses applied on the aneurysm wall, leading to early rupture at smaller sizes. A flow dynamics study conducted by Liou et al. demonstrated that small-sized saccular aneurysms arising at branching points are subjected to greater impinging forces based on laser-Doppler velocimetry measurements and flow visualizations (25). In addition, intra-aneurysmal flow dynamics are considerably influenced by geometric parameters such as the neck width and the branching angle of bifurcation aneurysms (38). The findings of the current study could inform the endovascular management of bifurcation or EW aneurysms with large branching angles by deploying a stent extending from the PV toward one of the daughter vessels, thus decreasing the branching angle.

Limitations

The limitations of this study include its retrospective nature and relatively small sample size. Although a total of 250 ruptured IAs were explored, the sample sizes within each subgroup (SW, SWB, and EW aneurysms) were still relatively small. Therefore, more studies are needed to support our conclusions. Another limitation is the vessel narrowing, which could be contributed to by vasospasm caused by a ruptured aneurysm, potentially altering our measurements. Additionally, it is still unclear whether peripheral vascular morphology alters during the development of aneurysms or whether differences in vascular morphology cause hemodynamic alterations that subsequently cause aneurysm growth and rupture. Answering this question will require further research with larger cohorts.

CONCLUSION

Geometrical factors such as PV curvature angle, aneurysm neck width, and distal narrowing of the PV could affect the risk of growth and rupture of SW and SWB aneurysms. A wider branching angle could be considered a contributor to the early

rupture of EW aneurysms. Neck width could be significantly related to the growth and rupture of both SW and EW IAs.

Declarations

Funding: This research did not receive any specific grant from funding agencies in the public, commercial, or not-for-profit sectors.

Availability of data and materials: The datasets generated and/or analyzed during the current study are available from the corresponding author by reasonable request.

Disclosure: The authors declare no competing interests.

AUTHORSHIP CONTRIBUTION

Study conception and design: ARS, AH, OA, AS, MA, WA, AE, TH
Data collection: TH, ARS, AH
Analysis and interpretation of results: TH, OA,
Draft manuscript preparation: ARS
Critical revision of the article: AS, MA, AE, WA
All authors (ARS, AH, OA, AS, MA, WA, AE, TH) reviewed the results and approved the final version of the manuscript.

REFERENCES

1. Antonov A, Kono K, Greim-Kuczewski K, Hippelheuser JE, Lauric A, Malek AM: Proximal stenosis is associated with rupture status in middle cerebral artery aneurysms. World Neurosurg 109:e835-e844, 2018. https://doi.org/10.1016/j.wneu.2017.10.108
2. Baharoglu MI, Lauric A, Safain MG, Hippelheuser J, Wu C, Malek AM: Widening and high inclination of the middle cerebral artery bifurcation are associated with presence of aneurysms. Stroke 45:2649-2655, 2014. https://doi.org/10.1161/STROKEAHA.114.005393
3. Baharoglu MI, Schirmer CM, Hoit DA, Gao BL, Malek AM: Aneurysm inflow-angle as a discriminant for rupture in sidewall cerebral aneurysms: Morphometric and computational fluid dynamic analysis. Stroke 41:1423-1430, 2010. https://doi.org/10.1161/STROKEAHA.109.570770
4. Bhogal P, AlMatter M, Hellstern V, Ganslandt O, Bäzner H, Henkes H, Pérez MA: Difference in aneurysm characteristics between ruptured and unruptured aneurysms in patients with multiple intracranial aneurysms. Surg Neurol Int 9:1, 2018. https://doi.org/10.4103/SNI.SNI_339_17
5. Cebral JR, Mut F, Weir J, Putman CM: Association of hemodynamic characteristics and cerebral aneurysm rupture. AJNR Am J Neuroradiol 32:264-270, 2011. https://doi.org/10.3174/ajnr.A2274
6. Charbel FT, Seyfried D, Mehta B, Dujovny M, Ausman JI: Dominant A: Angiographic and clinical correlations with anterior communicating artery aneurysms. Neurol Res 13:253-256, 1991. https://doi.org/10.1080/01616412.1991.11740001
7. Connolly ESJ, Rabinstein AA, Carhuapoma JR, Derdeyn CP, Dion J, Higashida RT, Hoh BL, Kirkness CJ, Naidech AM, Ogilvy CS, Patel AB, Thompson BG, Vespa P: Guidelines for the management of aneurysmal subarachnoid hemorrhage: A guideline for healthcare professionals from the American Heart Association/american Stroke Association. Stroke 43:1711–1737, 2012. https://doi.org/10.1161/STR.0b013e3182587839
8. Dhar S, Tremmel M, Mocco J, Kim M, Yamamoto J, Siddiqui AH, Hopkins LN, Meng H: Morphology parameters for intracranial aneurysm rupture risk assessment. Neurosurgery 63:185-187, 2008. https://doi.org/10.1227/01.NEU.0000316847.64140.81
9. Edjlali M, Gentric JC, Régent-Rodriguez C, Trystram D, Hassen W Ben, Lion S, Nataf F, Raymond J, Wieben O, Turski P, Meder JF, Oppenheim C, Naggara O: Does aneurysmal wall enhancement on vessel wall MRI Help to distinguish stable from unstable intracranial aneurysms? Stroke 45:3704-3706, 2014. https://doi.org/10.1161/STROKEAHA.114.006626
10. Fernandez Zubillaga A, Guglielmi G, Viñuela F, Duckwiler GR: Endovascular occlusion of intracranial aneurysms with electrically detachable coils: Correlation of aneurysm neck size and treatment results. AJNR Am J Neuroradiol 15:815-820, 1994.
11. Foutrakis GN, Yonas H, Sclabassi RJ: Saccular aneurysm formation in curved and bifurcating arteries. AJNR Am J Neuroradiol 20:1309-1317, 1999.
12. Gao B, Baharoglu MI, Malek AM: Angular remodeling in single stent-assisted coiling displaces and attenuates the flow impingement zone at the neck of intracranial bifurcation aneurysms. Neurosurgery 72:739-748; discussion 748, 2013. https://doi.org/10.1227/NEU.0b013e318286fab3
13. Hassan T, Timofeev E V, Saito T, Shimizu H, Ezura M, Matsumoto Y, Takayama K, Tominaga T, Takahashi A: A proposed parent vessel geometry-based categorization of saccular intracranial aneurysms: computational flow dynamics analysis of the risk factors for lesion rupture. J Neurosurg 103:662–680, 2005. https://doi.org/10.3171/jns.2005.103.4.0662
14. Hendricks BK, Yoon JS, Yaeger K, Kellner CP, Mocco J, De Leacy RA, Ducruet AF, Lawton MT, Mascitelli JR: Wide-neck aneurysms: Systematic review of the neurosurgical literature with a focus on definition and clinical implications. J Neurosurg 133:159-165, 2019. https://doi.org/10.3171/2019.3.JNS183160
15. Ishii A, Chihara H, Kikuchi T, Arai D, Ikeda H, Miyamoto S: Contribution of the straightening effect of the parent artery to decreased recanalization in stent-assisted coiling of large aneurysms. J Neurosurg 127:1063-1069, 2017. https://doi.org/10.3171/2016.9.JNS16501
16. Janot K, Fahed R, Rouchaud A, Zuber K, Boulouis G, Forestier G, Mounayer C, Piotin M: Parent artery straightening after flow-diverter stenting improves the odds of aneurysm occlusion. AJNR Am J Neuroradiol 43:87-92, 2022. https://doi.org/10.3174/ajnr.A7350
17. Kashiwazaki D, Kuroda S: Size ratio can highly predict rupture risk in intracranial small (<5 mm) aneurysms. Stroke 44:2169-2173, 2013. https://doi.org/10.1161/STROKEAHA.113.001138
18. Kono K, Fujimoto T, Terada T: Proximal stenosis may induce initiation of cerebral aneurysms by increasing wall shear stress and wall shear stress gradient. Int J Numer Method Biomed Eng 30:942-950, 2014. https://doi.org/10.1002/cnm.2637
19. Kono K, Masuo O, Nakao N, Meng H: De novo cerebral aneurysm formation associated with proximal stenosis. Neurosurgery 73:E1080-1090, 2013. https://doi.org/10.1227/NEU.0000000000000065

20. Lauric A, Greim-Kuczewski K, Antonov A, Dardik G, Magida JK, Hippelheuser JE, Kono K, Malek AM: Proximal parent vessel tapering is associated with aneurysm at the middle cerebral artery bifurcation. Neurosurgery 84:1082-1089, 2019. https://doi.org/10.1093/neuros/nyy152
21. Lauric A, Safain MG, Hippelheuser J, Malek AM: High curvature of the internal carotid artery is associated with the presence of intracranial aneurysms. J Neurointerv Surg 6:733-739, 2014. https://doi.org/10.1136/neurintsurg-2013-010987
22. Lauric A, Silveira L, Lesha E, Breton JM, Malek AM: Aneurysm presence at the anterior communicating artery bifurcation is associated with caliber tapering of the A1 segment. J Neurosurg 136:1694-1704, 2022. https://doi.org/10.3171/2021.5.JNS204389
23. Lazareska M, Aliji V, Stojovska-Jovanovska E, Businovska J, Mircevski V, Kostov M, Papazova M: Endovascular treatment of wide neck aneurysms. open access maced. J Med Sci 6:2316–2322, 2018. https://doi.org/10.3889/oamjms.2018.443
24. Lin N, Ho A, Charoenvimolphan N, Frerichs KU, Day AL, Du R: Analysis of morphological parameters to differentiate rupture status in anterior communicating artery aneurysms. PLoS One 8:e79635, 2013. https://doi.org/10.1371/journal.pone.0079635
25. Liou TM, Chang WC, Liao CC: Experimental study of steady and pulsatile flows in cerebral aneurysm model of various sizes at branching site. J Biomech Eng 119:325-332, 1997. https://doi.org/10.1115/1.2796097
26. Lv N, Wang C, Karmonik C, Fang Y, Xu J, Yu Y, Cao W, Liu J, Huang Q: Morphological and hemodynamic discriminators for rupture status in posterior communicating artery aneurysms. PLoS One 11:e0149906, 2016. https://doi.org/10.1371/journal.pone.0149906
27. Meng H, Tutino VM, Xiang J, Siddiqui A: High WSS or low WSS? Complex interactions of hemodynamics with intracranial aneurysm initiation, growth, and rupture: Toward a unifying hypothesis. AJNR Am J Neuroradiol 35:1254-1262, 2014. https://doi.org/10.3174/ajnr.A3558
28. Meng H, Wang Z, Kim M, Ecker RD, Hopkins LN: Saccular aneurysms on straight and curved vessels are subject to different hemodynamics: Implications of intravascular stenting. AJNR Am J Neuroradiol 27:1861-1865, 2006.
29. Miyata T, Kataoka H, Shimizu K, Okada A, Yagi T, Imamura H, Koyanagi M, Ishibashi R, Goto M, Sakai N, Hatano T, Chin M, Iwasaki K, Miyamoto S: Predicting the growth of middle cerebral artery bifurcation aneurysms using differences in the bifurcation angle and inflow coefficient. J Neurosurg 138:1357-1365, 2023. https://doi.org/10.3171/2022.8.JNS22597
30. Nader-Sepahi A, Casimiro M, Sen J, Kitchen ND: Is aspect ratio a reliable predictor of intracranial aneurysm rupture? Neurosurgery 54:1343-1348, 2004. https://doi.org/10.1227/01.neu.0000124482.03676.8b
31. Neyazi B, Swiatek VM, Skalej M, Beuing O, Stein KP, Hattingen J, Preim B, Berg P, Saalfeld S, Sandalcioglu IE: Rupture risk assessment for multiple intracranial aneurysms: Why there is no need for dozens of clinical, morphological and hemodynamic parameters. Ther Adv Neurol Disord 14:13, 2020. https://doi.org/10.1177/1756286420966159
32. Piccinelli M, Bacigaluppi S, Boccardi E, Ene-Iordache B, Remuzzi A, Veneziani A, Antiga L: Geometry of the internal carotid artery and recurrent patterns in location, orientation, and rupture status of lateral aneurysms: An image-based computational study. Neurosurgery 68:1270-1285; discussion 1285, 2011. https://doi.org/10.1227/NEU.0b013e31820b5242
33. Raghavan ML, Ma B, Harbaugh RE: Quantified aneurysm shape and rupture risk. J Neurosurg 102:355-362, 2005. https://doi.org/10.3171/jns.2005.102.2.0355
34. Rahman M, Smietana J, Hauck E, Hoh B, Hopkins N, Siddiqui A, Levy EI, Meng H, Mocco J: Size ratio correlates with intracranial aneurysm rupture status: A prospective study. Stroke 41:916-920, 2010. https://doi.org/10.1161/STROKEAHA.109.574244
35. Rostamian A, Fallah K, Rostamiyan Y: Reduction of rupture risk in ICA aneurysms by endovascular techniques of coiling and stent: Numerical study. Scientific Reports 13:1–11, 2023. https://doi.org/10.1038/s41598-023-34228-2
36. Sámano A, Ishikawa T, Moroi J, Yamashita S, Suzuki A, Yasui N: Ruptured de Novo Posterior Communicating Artery Aneurysm Associated with Arteriosclerotic Stenosis of the Internal Carotid Artery at the Supraclinoid Portion, Vol: 2, Surgical Neurology International. United States, 2011:35. https://doi.org/10.4103/2152-7806.78243
37. Saqr KM, Rashad S, Tupin S, Niizuma K, Hassan T, Tominaga T, Ohta M: What does computational fluid dynamics tell us about intracranial aneurysms? A meta-analysis and critical review. J Cereb Blood Flow Metab 40:1021-1039, 2020. https://doi.org/10.1177/0271678X19854640
38. Shojima M, Oshima M, Takagi K, Hayakawa M, Katada K, Morita A, Kirino T: Numerical simulation of the intra-aneurysmal flow dynamics. Interv Neuroradiol 12:49-52, 2006. https://doi.org/10.1177/15910199060120S105
39. Sunohara T, Imamura H, Goto M, Fukumitsu R, Matsumoto S, Fukui N, Oomura Y, Akiyama T, Fukuda T, Go K, Kajiura S, Shigeyasu M, Asakura K, Horii R, Sakai C, Sakai N: Neck location on the outer convexity is a predictor of incomplete occlusion in treatment with the pipeline embolization device: Clinical and angiographic outcomes. Am J Neuroradiol 42:119-125, 2021. https://doi.org/10.3174/AJNR.A6859
40. Tan J, Zhu H, Huang J, Ouyang HY, Pan X, Zhao Y, Li M: The association of morphological differences of middle cerebral artery bifurcation and aneurysm formation: A systematic review and meta-analysis. World Neurosurg 167:17-27, 2022. https://doi.org/10.1016/j.wneu.2022.08.075
41. Texakalidis P, Hilditch CA, Lehman V, Lanzino G, Pereira VM, Brinjikji W: Vessel wall imaging of intracranial aneurysms: Systematic review and meta-analysis. World Neurosurg 117:453-458.e1, 2018. https://doi.org/10.1016/J.WNEU.2018.06.008
42. The International Study of Unruptured Intracranial Aneurysms Investigators: Unruptured intracranial aneurysms--risk of rupture and risks of surgical intervention. N Engl J Med 339:1725–1733, 1998. https://doi.org/10.1056/NEJM199812103392401
43. Tütüncü F, Schimansky S, Baharoglu MI, Gao B, Calnan D, Hippelheuser J, Safain MG, Lauric A, Malek AM: Widening of the basilar bifurcation angle: Association with presence of intracranial aneurysm, age, and female sex. J Neurosurg 121:1401-1410, 2014. https://doi.org/10.3171/2014.8.JNS1447

44. Ujiie H, Tachibana H, Hiramatsu O, Hazel AL, Matsumoto T, Ogasawara Y, Nakajima H, Hori T, Takakura K, Kajiya F: Effects of size and shape (aspect ratio) on the hemodynamics of saccular aneurysms: A possible index for surgical treatment of intracranial aneurysms. Neurosurgery 45:119-130, 1999. https://doi.org/10.1097/00006123-199907000-00028
45. Ujiie H, Tamano Y, Sasaki K, Hori T: Is the aspect ratio a reliable index for predicting the rupture of a saccular aneurysm? Neurosurgery 48:493-495, 2001. https://doi.org/10.1097/00006123-200103000-00007
46. Waihrich E, Clavel P, Mendes G, Iosif C, Kessler IM, Mounayer C: Influence of anatomic changes on the outcomes of carotid siphon aneurysms after deployment of flow-diverter stents. Neurosurgery 83:1226-1233, 2018. https://doi.org/10.1093/neuros/nyx618
47. Waqas M, Chin F, Rajabzadeh-Oghaz H, Gong AD, Rai HH, Mokin M, Vakharia K, Dossani RH, Meng H, Snyder KV, Davies JM, Levy EI, Siddiqui AH: Size of ruptured intracranial aneurysms: A systematic review and meta-analysis. Acta Neurochir (Wien) 162:1353-1362, 2020. https://doi.org/10.1007/s00701-020-04291-z
48. Wiebers DO, Whisnant JP, Huston J 3rd, Meissner I, Brown RDJ, Piepgras DG, Forbes GS, Thielen K, Nichols D, O'Fallon WM, Peacock J, Jaeger L, Kassell NF, Kongable-Beckman GL, Torner JC: Unruptured intracranial aneurysms: Natural history, clinical outcome, and risks of surgical and endovascular treatment. Lancet 362:103-110, 2003. https://doi.org/10.1016/s0140-6736(03)13860-3
49. Wills S, Ronkainen A, van der Voet M, Kuivaniemi H, Helin K, Leinonen E, Frösen J, Niemela M, Jääskeläinen J, Hernesniemi J, Tromp G: Familial intracranial aneurysms: An analysis of 346 multiplex Finnish families. Stroke 34:1370-1374, 2003. https://doi.org/10.1161/01.STR.0000072822.35605.8B
50. Xiang J, Natarajan SK, Tremmel M, Ma D, Mocco J, Hopkins LN, Siddiqui AH, Levy EI, Meng H: Hemodynamic-morphologic discriminants for intracranial aneurysm rupture. Stroke 42:144-152, 2011. https://doi.org/10.1161/STROKEAHA.110.592923
51. Yamaguchi S, Ito O, Osaki M, Haruyama H, Nitta T, Sayama T, Arakawa S, Iihara K: Narrowing of the angle of the parent artery after coil embolization increases the risk for aneurysm recurrence. Clin Neurol Neurosurg 203:106568, 2021. https://doi.org/10.1016/j.clineuro.2021.106568
52. Yerramilli SK, Kokula P, Gupta SK, Radotra BD, Aggarwal A, Aggarwal D, Chatterjee D: Connective tissue abnormalities in patients with ruptured intracranial aneurysms and no known systemic connective tissue disorder. World Neurosurg 141:e829-e835, 2020. https://doi.org/10.1016/j.wneu.2020.06.047
53. Zuurbier CCM, Molenberg R, Mensing LA, Wermer MJH, Juvela S, Lindgren AE, Jääskeläinen JE, Koivisto T, Yamazaki T, Uyttenboogaart M, van Dijk JMC, Aalbers MW, Morita A, Tominari S, Arai H, Nozaki K, Murayama Y, Ishibashi T, Takao H, Gondar R, Bijlenga P, Rinkel GJE, Greving JP, Ruigrok YM: Sex difference and rupture rate of intracranial aneurysms: An individual patient data meta-analysis. Stroke 53:362-369, 2022. https://doi.org/10.1161/STROKEAHA.121.035187